HHS Public Access

Author manuscript

Nat Cell Biol. Author manuscript; available in PMC 2019 October 01.

Published in final edited form as:

Nat Cell Biol. 2019 April ; 21(4): 420–429. doi:10.1038/s41556-019-0301-x.

An Opsin 5-dopamine pathway mediates light-dependent vascular development in the eye

Minh-Thanh T. Nguyen[1,3], **Shruti Vemaraju**[1,3], **Gowri Nayak**[1,3], **Yoshinobu Odaka**[1,3], **Ethan D. Buhr**[5], **Nuria Alonzo**[1], **Uyen Tran**[1], **Mathew Batie**[11], **Brian A. Upton**[1,3], **Martin Darvas**[7], **Zbynek Kozmik**[12], **Sujata Rao**[10], **Rashmi S. Hegde**[2], **P. Michael Iuvone**[8,9], **Russell N. Van Gelder**[5,6,7], and **Richard A. Lang**[1,2,3,4,*]

[1]The Visual Systems Group, Abrahamson Pediatric Eye Institute, Division of Pediatric Ophthalmology, Cincinnati Children's Hospital Medical Center, Cincinnati, OH 45229, USA

[2]Division of Developmental Biology, Cincinnati Children's Hospital Medical Center, Cincinnati, OH 45229, USA

[3]Center for Chronobiology, Cincinnati Children's Hospital Medical Center, Cincinnati, OH 45229, USA

[4]Department of Ophthalmology, University of Cincinnati, College of Medicine, Cincinnati, OH 45229, USA

[5]Department of Ophthalmology, University of Washington Medical School, Seattle, WA 98104, USA

[6]Department of Biological Structure, University of Washington Medical School, Seattle, WA 98104, USA

[7]Department of Pathology, University of Washington Medical School, Seattle, WA 98104, USA

[8]Department of Ophthalmology, Emory University School of Medicine, Atlanta, GA 30322

[9]Department of Pharmacology, Emory University School of Medicine, Atlanta, GA 30322

[10]Ophthalmic Research, Cole Eye Institute, Cleveland Clinic, Cleveland, OH 44195

[11]Clinical Engineering, Cincinnati Children’s Hospital Medical Center, Cincinnati, OH 45229, USA

[*]Correspondence should be addressed to: **Richard A. Lang**, Visual Systems Group, Center for Chronobiology, Division of Pediatric Ophthalmology, Cincinnati Children's Hospital Medical Center, 3333 Burnet Avenue, Cincinnati, OH 45229, Tel: 513-636-2700 (Office), 513-803-2230 (Assistant), Fax: 513-636-4317. Richard.Lang@cchmc.org.

Author Contributions

M-TN, SV, GN, YO, EDB, BAU, NA, SR and UT performed experimental analysis. MB designed and built the required lighting systems. MD and ZK provided essential tools. M-TN, SV, GN, YO, EB, SR, RSH, PMI and RNVG designed experiments and provided coordinating leadership within the collaborative group. M-TN, SV, GN EB, PMI, RNVG and RAL wrote the paper. RAL designed experimental analysis and provided overall project leadership.

Competing Interests

The authors declare no competing interests.

[12]Institute of Molecular Genetics, Academy of Sciences of the Czech Republic, Videnska 1083, 14220 Praha 4, Czech Republic

Abstract

During mouse postnatal eye development, the embryonic hyaloid vascular network regresses from the vitreous as an adaption for high acuity vision. This process occurs with precisely controlled timing. Here we show that an Opsin 5 (OPN5, Neuropsin)-dependent retinal light response regulates vascular development in the postnatal eye. In *Opn5* null mice hyaloid vessels regress precociously. We demonstrate that 380 nm light stimulation *via* OPN5 and VGAT (the vesicular GABA/glycine transporter) in retinal ganglion cells enhances activity of inner retinal DAT/SLC6A3 (a dopamine reuptake transporter) and thus suppresses vitreal dopamine. In turn, dopamine acts directly on hyaloid vascular endothelial cells to suppress activity of VEGFR2 and promote hyaloid vessel regression. With OPN5 loss-of-function, vitreous dopamine is elevated and results in premature hyaloid regression. These investigations identify violet light as a developmental timing cue that, via an OPN5-dopamine pathway, regulates optic axis clearance in preparation for visual function.

Photons from the sun reach our planet at high flux. In response, organisms have evolved detection systems that decode light information for adaptive advantage. Examples from mammals include the visual system[1], where photons bouncing off an object are detected to decode object identity, and the circadian system, where the 24 hour light cycle entrains time-of-day dependent physiology[2,3]. Most light detectors in metazoans are opsins[4,5], a class of G-protein coupled receptors that convert the energy of a photon into a cellular signalling response. Rhodopsin, the opsin of mammalian rod photoreceptors, is a well-characterized example of a visual opsin[6,7] while melanopsin (Opsin 4, OPN4) has a central role in circadian clock photoentrainment[8-10]. Neuropsin (Opsin 5, OPN5) is another opsin family member. Relatively little is known about OPN5 except that it responds to violet light wavelengths (λ_{max} of 380 nm)[11-15], regulates seasonal breeding behaviour in birds[16] and the activity cycle in mice[17] but also mediates photoentrainment of the retinal circadian clock[18]. Here we have investigated OPN5 function in development of the mouse eye and shown, like the above examples, that it is required for normal biological timing. In this case, OPN5 is required for a light response that regulates vascular regression timing.

Results

Opn5 is expressed in a retinal ganglion cell subset.

Opn5 is expressed in retinal ganglion cells (RGCs) in adult mice[18]. To further assess the features of *Opn5*-expressing cells, we combined an $Opn5^{cre}$ allele (Supplementary Fig. 1) with *Ai14*, a tdTomato expressing cre reporter. According to labelling with multiple markers (Supplementary Figure 2) the overall architecture of the *Opn5* null retina is unchanged. In P5 retinal flat mounts, $Opn5^{cre}$; *Ai14* cells were at relatively low density throughout the inner retina (Fig. 1a). In P12 calretinin-labelled cryosections , *Opn5* expressing cell bodies were in the ganglion cell layer (Fig. 1c, d, GCL). At P5, *Ai14* expressing processes were immature (Fig. 1a) but at P12 were prominent and observed as bundles within the nerve fibre

layer (NFL) and within several laminations of the inner plexiform layer (Fig. 1c, d, IPL, S1-S5). These morphological features are consistent with the characteristics of RGCs.

Melanopsin antibody labelling in *Opn5*^{cre}; *Ai14* retinae indicated that OPN4 and *Opn5* are expressed in distinct RGC subsets. At P5, the density of *Opn5*^{cre}*; Ai14* and OPN4-labelled cells was similar (Fig. 1b). At P12 (Fig. 1e-h) co-labelling again showed that largely, melanopsin and *Opn5*^{cre}; *Ai14* cells were two distinct subsets. Prominent bundles of axons from *Opn5* and OPN4 RGCs are cofasciculated (Fig. 1e-g). Rare co-labelled cells were identified (Fig. 1e, h, about 50 cells per retina) but could result from cre lineage marking over-sampling[19]. At P24, *Opn5*^{cre}; *Brainbow*[20] labelled retinal cells (Fig. 1i, j) have the appearance of mature RGCs with extensive dendritic arbours and axons. Brain cryosections from *Opn5*^{cre}*; Ai14* mice showed axons in the optic tracts, lateral geniculate nucleus and superior colliculus as might be expected for RGCs. Labelling of *Opn5*^{cre}*; Ai6* retinae at P8 with the RGC marker RBPMS[21] and the RGC/amacrine cell marker Calretinin[22] provided evidence that *Opn5* is expressed exclusively in RGCs (Supplementary Figure 3).

Normal hyaloid vessel regression timing requires *Opn5* and violet light.

We have previously shown that light stimulation of melanopsin (*Opn4*) regulates hyaloid vessel regression and retinal angiogenesis[23]. Prompted by this, we assessed hyaloid regression in the *Opn5* null mouse. At P1, *Opn5* null mice showed normal hyaloid vessel numbers (Fig. 2a, b, g, h) and normal vessel cellularity (Fig. 2c, d, control, 13.3±1.2, *Opn5* null, 13.2±1.6 nuclei/100 μm length, p=0.92). At P8, *Opn5* null mice had fewer hyaloid vessels (Fig. 2e-h) indicating precocious regression. This phenotype is unique as all hyaloid phenotypes described so far[24], including that of the *Opn4* null mouse[23], show hyaloid persistence. Precocious hyaloid regression in the *Opn5* null mouse is best illustrated when vessel numbers are quantified over a P1-P8 time-course (Fig. 2g, h, blue line) and compared with the control (Fig. 2g, h, grey line) and the *Opn4* null (Fig. 2h, green line). When *Opn5*^{fl} is conditionally deleted in the retina using *Chx10-cre* or *Rx-cre* precocious hyaloid regression is observed (Fig. 2i-k). Thus, OPN5 is required locally within retinal neurons to regulate hyaloid regression.

To mimic *Opn5* loss-of-function using lighting conditions, we raised mice from birth in the absence of the 380 nm wavelengths that maximally stimulate OPN5[11-14]. Control mice were raised in a light-dark cycle of “VBGR” lighting (violet (380 nm), blue (480 nm), green (520 nm) and red (630 nm)) and showed a typical hyaloid vessel number at P8 (Fig. 2l, and n, grey bar). By contrast, mice raised in “BGR” lighting that omitted violet light showed precocious hyaloid regression (Fig. 2m, and n, blue bar). This phenocopies the *Opn5* null and is consistent with a model in which 380 nm photons stimulate OPN5 to suppress hyaloid vessel regression.

A light-OPN5 pathway regulates dopamine levels in the eye.

In *Opn4* null mice, elevated levels of VEGFA explain hyaloid vessel persistence[23]. Assessment of the levels of VEGFA and its inhibitor FLT1[25] in the vitreous of *Opn5* null mice indicated no change (Supplementary Fig. 4d, e). This suggested that the OPN5-light response pathway regulated hyaloid regression by a distinct mechanism. In the *Opn5* null

retina, we noted an unusual labelling pattern for tyrosine hydroxylase (TH). In WT retina at P8, TH immunoreactivity was faint and largely restricted to the perinuclear region of a subset of amacrine cells (Fig. 3a, b). In *Opn5* null mice, TH labelling was stronger and prominent in cell processes (Fig. 3c, d). Elevated intensity of TH labelling in the *Opn5* null retina was also evident at P15 when dopaminergic amacrine cells are more fully developed (Fig. 3e, f). TH is the rate-limiting enzyme that mediates the first step in the biosynthesis of dopamine. Since TH levels are under feedback regulation[26], these data suggested that dopamine levels might be modulated in the *Opn5* null eye. Interestingly, dopamine is known to have *in vitro* anti-vascular activity via suppression of VEGFR2 signalling[27,28]. This meant that *Opn5*-dependent regulation of dopamine could be an explanation for *Opn5*-dependent regulation of hyaloid regression. Thus, we hypothesized that OPN5-dependent release of dopamine from the retina promoted hyaloid vessel regression by direct signalling.

Dopaminergic amacrine cells that express TH develop in the first few days after birth in the mouse[29]. This also means that normally, dopamine levels in the retina climb rapidly after birth[29]. Using ELISA quantification, we confirmed that retinal dopamine levels rise over a P2 to P8 time-course (Fig. 3g). Dopamine in solubilized retinal tissue is primarily from intracellular stores[30]. ELISA quantification showed that dopamine levels in the vitreous, where the hyaloid vessels reside, also rise over the postnatal period (Fig. 3h). In adult mice, dopamine levels in the eye are light-regulated[31,32,33,34]. To evaluate this possibility for neonatal mice, we quantified vitreous dopamine over a postnatal time-course of LD and DD lighting. At P4 and P6, vitreal dopamine levels were significantly elevated in DD (Fig. 3i) indicating that postnatally, light stimulation normally suppresses vitreal dopamine. To determine whether light-regulated dopamine might be a consequence of OPN5 activity, we harvested retina and vitreous from an *Opn5* allelic series at P6 and quantified dopamine (Fig. 3j, k). This showed that *Opn5* homozygote null mice had lower levels of intracellular dopamine in the retina (Fig. 3j), but elevated levels in the vitreous (Fig. 3k). These data indicate that dopamine in both compartments is regulated by OPN5.

A light-OPN5 pathway suppresses dopamine release to the vitreous by enhancing DAT activity.

The biological effects of dopamine are regulated by its release, signalling and reuptake[35,36]. A key regulator of uptake, and thus a good candidate for an OPN5-dependent activity, is the dopamine transporter DAT/SLC6A3[36,37]. Threonine 53 of DAT is phosphorylated and enhances the rate of dopamine uptake by DAT[37]. This activation marker can be detected with a phospho-specific antibody[37]. Basal phosphorylation stoichiometry of T53-DAT is typically 50% but is increased by stimuli that elevate dopamine uptake[37]. To determine whether phospho-T53-DAT levels were regulated by light and were OPN5-dependent, we labelled retinal cryosections from cohorts of P8 littermate $Opn5^{+/+}$ and $Opn5^{-/-}$ mice after they were dark-adapted followed by ±30 minutes of 380 nm light at 1×10^{12} photons/cm^2/sec. Labelling for phospho-T53-DAT was found throughout the inner plexiform layer (IPL) and nerve fibre layer (NFL) of all samples (Fig. 4a-d). Phospho-T53-DAT signal was quantified by averaging pixel intensity across horizontal pixel rows of images aligned like those shown (Fig. 4a-d), generating intensity profiles (Fig. 4e, grey and blue profiles) and calculating area under the peaks (indicated by the grey vertical dashed lines in Fig. 4e and f).

This revealed that for the IPL (Fig. 4g, grey and blue bars) but not for the NFL (Fig. 4h, grey and blue bars), phospho-T53-DAT signal was significantly increased in response to 380 nm light.

To determine whether light induction of phospho-T53-DAT signal was OPN5-dependent, we performed the same analysis in *Opn5* null mice (Fig. 4c, d, f-h). This revealed that in the *Opn5* null retina, phospho-T53-DAT signal for the IPL did not elevate in response to light exposure (Fig. 4g, orange and red bars) indicating OPN5-dependence. Interestingly, in the NFL, *Opn5* null mice have a lower level of phospho-T53-DAT independent of light exposure (Fig. 4h, compare grey bar and orange bar). However, this low level of phospho-T53-DAT can be rescued by light exposure (Fig. 4h, compare orange and red bars). This indicates that NFL phospho-T53-DAT levels are regulated both by OPN5 (negatively, light-independent) and by a distinct light response pathway (positively). Though we do not currently understand the pathway for positive regulation of phospho-T53-DAT in the NFL (other opsins are obvious candidates), it serves as a useful internal control to show that the *Opn5* null retina can be light responsive. An immunoblot detecting phospho-T53-DAT in total solubilized retina from the light phase (Fig. 4i) revealed that overall, the level is lower in the *Opn5* null, suggesting that NFL phospho-T53-DAT is the smaller proportion of the total. Collectively, analysis of T53-DAT indicates that OPN5 is required for a light-dependent upregulation within the IPL. Since T53 phosphorylated DAT sequesters dopamine with higher efficiency, this finding is consistent with a model in which loss of OPN5 function results in diminished dopamine uptake by DAT/SLC6A3, and thus elevated levels of vitreal dopamine.

Inhibition of DAT/SLC6A3 promotes hyaloid regression in an *Opn5*-dependent manner.

To determine whether DAT had a functional role in the regulation of hyaloid regression *in vivo*, we took advantage of the DAT inhibitor GBR12909[38]. Based on data showing that dopamine signalling can suppress VEGFR2 activation via the phosphatase SHP2[28] we would predict that suppressing DAT activity would elevate dopamine levels in the eye and thus should counter the consequences of dark rearing because the latter elevates levels of VEGFA[39]. To test this, we compared the effects of P1-P8 GBR12909 injection on hyaloid vessel regression in C57BL/6J mice raised either in normal (LD) lighting or in constant darkness (DD). This showed that GBR12909 had no significant effect on mice raised in normal lighting (Fig. 4j, LD) but could reverse the hyaloid vessel persistence resulting from dark rearing (Fig. 4j, DD). This shows that DAT activity is an important light-dependent regulator of hyaloid vessel regression.

To assess DAT activity in OPN5-dependent regulation of hyaloid regression, we injected GBR12909 daily from P1-P8 into *Opn5*$^{+/+}$, *Opn5*$^{+/-}$, and *Opn5*$^{-/-}$ mouse pups. Quantification of hyaloid vessels at P8 showed that wild type (WT) mice did not respond significantly (Fig. 4k) but that in heterozygote mice, GBR12909 produced a precocious hyaloid regression equivalent to the *Opn5* homozygote phenotype (Fig. 4k). GBR12909 produced no change in homozygote mice (Fig. 4k). Inhibitor activity may be buffered by the intact feedback regulation of the WT mouse[40]. However, in *Opn5* heterozygote mice, where dopamine levels are elevated (Fig. 3k) and feedback regulation may be compromised, the DAT inhibitor was able to convert the hyaloid phenotype from normal to precocious

regression. It is likely that the inhibitor produces no effect in the *Opn5* homozygote because endogenous vitreal dopamine is already high (Fig. 3k) and signalling activity may be close to maximal. These data indicate a finely balanced interaction between OPN5 and DAT that is consistent with OPN5-dependent regulation of DAT activity via phosphorylation.

VGAT in OPN5 RGCs is required for regulation of phospho-T53-DAT and hyaloid regression.

Glutamate, γ-aminoburyric acid (GABA) and glycine are neurotransmitters important for visual function. In the adult mouse, glutamate is used as an excitatory neurotransmitter by canonical photoreceptors[41,42] and OPN4 RGCs[43]. GABA and glycine are inhibitory neurotransmitters and their receptors are detected in a variety of retinal neurons including amacrine cells and RGCs[42]. Glutamate and GABA/glycine are loaded into presynaptic vesicles by the VGLUT (vesicular glutamate transporter 2) and VGAT (vesicular GABA transporter) family of transporters, respectively. During mouse retinal development, VGAT is expressed soon after birth and precedes the expression of VGLUT2[44]. Loss-of-function of these transporters eliminates neurotransmitter activity[45,46]. To determine whether OPN5 RGCs might use one of these neurotransmitters for the vascular response pathway, we quantified hyaloid vessels in $Opn5^{cre}$ conditional deletion mutants of *Vglut2* and *Vgat*. Though deletion of $Vglut2^{fl}$ had no consequence (Fig. 5a) homozygous deletion of $Vgat^{fl}$ phenocopied the *Opn5* germ line null precocious hyaloid regression (Fig. 5b-f). Furthermore, the $Opn5^{cre/+}$ heterozygote showed no hyaloid phenotype, but $Opn5^{+/cre}$; $Vgat^{fl/+}$ mice showed a significant precocious regression (Fig. 5d, f). This transheterozygote phenotype is genetic evidence that *Opn5* and *Vgat* function in the same pathway and in the same cell type. If this is true, then we would predict that *Vgat* conditional deletion would, like *Opn5* loss-of-function, result in diminished levels of phospho-T53-DAT under lighted conditions. This was confirmed using immunofluorescence labelling of retina from $Opn5^{+/cre}$; $Vgat^{fl/+}$ (Fig. 5g, h) and $Opn5^{+/cre}$; $Vgat^{fl/fl}$ mice (Fig. 5i, j). These data suggest that OPN5 RGCs use VGAT to signal within the vascular regression pathway.

Dopamine has a direct action on hyaloid vascular endothelial cells (VECs) to promote hyaloid regression.

We have hypothesized that dopamine release from the neonatal retina is light- and OPN5-dependent and that dopamine then signals directly to hyaloid VECs to promote regression. To assess whether a retinal source of dopamine regulated hyaloid regression, we conditionally deleted a Th^{fl} allele. *Chx10-cre*[47], though effective for studies of TH function in adult mice[48] did not delete Th^{fl} efficiently during the postnatal period. However, *Rx-cre*[49] was effective (Fig. 6a, b) and resulted in a hyaloid vessel persistence (Fig. 6c-e) indicating that the active dopamine is produced locally in the retina.

To assess the involvement of dopamine receptors in hyaloid regression we first took advantage of SK38393, a receptor agonist[50]. SK38393 was injected daily into $Opn5^{+/+}$, $Opn5^{+/-}$, and $Opn5^{-/-}$ mouse pups from P1-P8. Though SK38393 had no significant effect on WT mice (Supplementary Fig. 4f), it produced precocious hyaloid regression in heterozygous mice (Supplementary Fig. 4f). SK38393 did not produce a significant reduction in hyaloid vessel numbers in *Opn5* null mice (Supplementary Fig. 4f). This pattern

of response is very similar to that observed with the DAT inhibitor (Fig. 4k). Again, this pattern of modulation is probably explained by the resilience of an intact dopamine feedback pathway in WT animals, the sensitized background of the heterozygote, and the already saturated level of dopamine signalling in the homozygote. Injection of two different dopamine receptor antagonists from P1-P8 in WT mice produced elevated numbers of hyaloid vessels (Supplementary Fig. 4g). Thus, pharmacological manipulations indicate that hyaloid vessel regression can be regulated both positively and negatively by dopamine receptor modulators.

One prediction of the hypothesis that retinal dopamine regulates hyaloid regression was that dopamine receptors would be expressed within the hyaloid vessels. Since DRD2 was implicated in suppression of VEGFR2 signalling[28], we focused on this member of the family. Vascular cells, but not hyaloid-associated myeloid cells, showed *Drd2-GFP* reporter expression (Fig. 6f, g). Furthermore, labelling with an anti-DRD2 antibody detected cells within the hyaloid vessels (Fig. 6h) and this was eliminated in the *Drd2$^{fl/fl}$; PDGFB-icreERT2* conditional deletion that targets VECs (Fig. 6i). These data show that DRD2 is expressed in hyaloid VECs.

In *Drd2$^{fl/fl}$; PDGFB-icreERT2* mice, the hyaloid vessels are persistent (Fig. 6j) but there are no quantifiable consequences for development of the superficial retinal vasculature (Supplementary Figure 5). This identifies hyaloid VECs as a dopamine responsive cell and indicates that dopamine signalling promotes hyaloid regression. A further prediction of the hypothesis is that in hyaloid VECs, dopamine signalling would suppress the activation of VEGFR2[51]. To test this, we performed immunblotting for VEGFR2 and the activated, phosphotyrosine-1173 form of VEGFR2, from both *Drd2$^{fl/fl}$* control and *Drd2$^{fl/fl}$; PDGFB-icreERT2* hyaloid vessels at P5. Pooling dissected hyaloids from 6 animals of each genotype allowed threshold detection of the pY1173-VEGFR2 in the control (Fig. 6k, left lane). To assess the reliability of comparative immunoblotting, we performed a three step, two-fold loading dilution and quantified immunoblot band intensities. Presented graphically, band intensities for VEGFR2, pY1173-VEGFR2 and β-tubulin showed high Pearson coefficients, indicating a linear relationship between lysate quantity and band intensity (Supplementary Fig. 6). When pY1173-VEGFR2 values were normalized to VEGFR2 (Fig. 6l), *Drd2$^{fl/fl}$; PDGFB-icreERT2* genotype values were much higher (Fig. 6l) consistent with the observed band intensities on the immunoblot (Fig. 6k). These data show that deletion of *Drd2* in hyaloid VECs permits elevated activation of VEGFR2 and indicates that normally, dopamine signalling suppresses VEGFR2 activity. In an additional test of this model, we assessed pY1173-VEGFR2 and pS473-AKT levels in the *Opn5* null. pY1173-VEGFR2 levels were lower in the hyaloid vessels of the *Opn5* null (Fig. 6m). In addition, across an allelic series, pS473-AKT levels were lower only in the *Opn5* homozygote, consistent with precocious hyaloid regression only in this genotype (Fig. 6n). Since dopamine levels are high in the *Opn5* null, these data are consistent with a model in which dopamine promotes hyaloid vessel regression by suppressing VEGFR2 activity and the downstream survival signalling mediated by AKT.

As a genetic test of the relationship between OPN5 and vascular signalling, we determined whether deletion of *Drd2* in VECs would reverse precocious hyaloid regression in the *Opn5*

null. We compared P8 hyaloid vessel numbers in mice of genotype *Opn5*$^{-/-}$, with *Opn5*$^{+/+}$; *PDGFB-icreERT2; Drd2*$^{fl/fl}$ and with *Opn5*$^{-/-}$; *PDGFB-icreERT2; Drd2*$^{fl/fl}$. This experiment confirmed the precocious regression of hyaloid vessels due to *Opn5* loss-of-function (Fig. 6o, p, and r, light blue bar) but showed that deletion of *Drd2* in VECs could switch the hyaloid phenotype to persistence (Fig. 6q, p, dark blue bar). This outcome establishes that *Opn5* and *Drd2* function in the same developmental pathway and have opposing influences on hyaloid regression.

One implication of immunoblotting data for pY1173-VEGFR2 (Fig. 6k) and the genetic analysis (Fig. 6o-r) is that a balance of VEGFA and dopamine signalling determines the fate of the hyaloid vessels. To determine whether we could demonstrate this balance at the level of receptor ligands, we designed a rescue experiment. We generated an elevated level of VEGFA activity, and thus hyaloid vessel persistence, by conditionally deleting the gene encoding the naturally occurring VEGFA inhibitor FLT1 in the retina. *Chx10-cre* deletion of *Flt1*$^{fl/fl}$ produces hyaloid persistence (Supplementary Figure 4a-c) but in this case, we used *Rx-cre* (Fig. 6s, t, v, light blue bar). To determine whether dopamine receptor signalling could reverse the hyaloid persistence, we injected (each day, from P1-P8) a littermate cohort of *Rx-cre; Flt1*$^{fl/fl}$ mice with the dopamine receptor agonist SKF38393. This resulted in a reversal of the hyaloid persistence (Fig. 6s-v), an outcome that illustrates the balance of VEGFA and dopamine signalling that regulates hyaloid regression.

Discussion

We have identified an unanticipated vascular development pathway in the eye. OPN5, an atypical opsin known to respond to near-UV photons[11-14], initiates the pathway response and functions postnatally (Fig. 5l). Dopamine, a broadly functional neurotransmitter and neuromodulator, is a signalling intermediate that is regulated by OPN5 and elicits a direct response in hyaloid VECs to limit VEGFR2 signalling via DRD2 (Fig. 5l). Based on OPN5- and light-dependent phosphorylation at threonine 53, and its pharmacological inhibition, our data also suggest that the dopamine transporter DAT/SLC6A3 is a key component of this pathway that normally suppresses levels of dopamine in the vitreous (Fig. 5l). In addition, the GABA transporter VGAT is implicated in OPN5 RGC signalling as its conditional deletion in OPN5 RGCs phenocopies the *Opn5* null precocious hyaloid regression and low phospho-T53-DAT. The light-OPN5-VGAT-dopamine-DRD2-VEGFR2-hyaloid pathway is thus characterized by two suppressive steps: light-OPN5 suppresses levels of dopamine in the vitreous while dopamine suppresses VEGFR2 signalling in the hyaloid vessels (Fig. 5l).

Light-dependent regulation of vitreal dopamine occurs against a backdrop of generally rising levels of dopamine in the postnatal eye. This means that while the function of dopamine is to promote hyaloid vessel regression, the effect of 380 nm photons and OPN5 is to suppress regression of the hyaloid vessels. It is likely that this has evolved as a mechanism to optimize the timing of hyaloid vessel regression and ensure that they remain functional postnatally until the superficial retinal vascular plexus is complete. We have previously shown that melanopsin (Opsin 4, OPN4) also mediates light-dependent vascular development in the eye[39] and suppresses VEGFA levels because it keeps retinal cellularity in check, and thus limits the oxygen demand that can elevate levels of VEGFA (Fig. 5l). The

crucial window for activation of the OPN4 response is in late gestation and requires a direct light stimulation of the mouse fetus[39]. Thus, the OPN4 and OPN5 response pathways use distinct mediators to regulate vascular development and, since they function at different stages of development, can be thought of as developmental timing cues (Fig. 5l). Notably, the spontaneous waves of neuronal activity that arise in the neonatal mouse retina[52,53] are partly dependent on OPN4 modulation of gap junctions that are, in turn, regulated by dopamine[54]. In the future, it will be interesting to assess the relationship of retinal wave activity to vascular development.

Neuropsin is highly conserved and we might anticipate that the pathway we describe (Fig. 5l) will be relevant to human biology. The latter steps in the pathway involving DRD2-dependent suppression of VEGFR2 activity may be an explanation for the observation that premature infants treated with dopamine (for hypotension) have a higher risk of retinopathy of prematurity (ROP)[55,56], a vascular overgrowth disease. We suggest that therapeutic dopamine promotes regression of the hyaloid vessels and thus exacerbates the hypoxia that leads to rebound vascular overgrowth. Furthermore, we have previously shown that the risk of ROP in premature infants is partly dependent on their season of gestation with short days and lower light exposure associated with higher risk[57]. It is possible that the OPN5-dopamine pathway is a component of this risk equation because insufficient light would be expected to result in elevated vitreal dopamine, precocious hyaloid regression and thus a more profound hypoxia in the premature eye. An understanding of the relationship between OPN4 and OPN5-dependent regulation of vascular development in the eye (Fig. 5l) raises the interesting possibility that premature infants at risk for ROP might be treated with a light therapy that differentially targets each pathway response. Finally, it has been proposed that both violet light in the 360–400 nm range[58] and dopamine[59] are key regulators of refractive development and that each can suppress progression to myopia. The current observations suggest that the OPN5-dopamine pathway is likely to be involved.

Materials and Methods

Mice

Animals were housed in a pathogen-free vivarium and all pharmacological treatments were in accordance with protocols approved by the Institutional Animal Care and Use Committee at Cincinnati Children's Hospital Medical Center. This study is compliant with all relevant ethical regulations regarding animal research. Day of birth is defined as P1. Genetically modified mice used in this study were: *Chx10cre* (*Tg(Chx10-EGFP/cre-ALPP)2Clc/J*) (Jax source #00515), *PdgfbicreER(T2)*[1], *Rxcre*[2], *Ai14* (Jax stock #007914), *Brainbow* (Jax stock #021227 *Brainbow 3.2*), *Drd2*^{EGFP} (*Tg(Drd2-EGFP)S118Gsat*)[3], *Drd2*^{loxp} (Jax stock #020631), *Flt1*^{flox} (Jax stock #02809 *Vegfr-1*^{flox}), *TH*^{flox} (Ref[4]), *Vglut2*^{fl} (Jax stock #012898), *Vgat*^{fl} (Jax stock #012897), *Opn4* (Ref[5]) and *Opn5*$^{tm1a(KOMP)Wtsi}$ that were generated from C57BL/6N ES cells obtained from KOMP (ES clone ID:KOMP-(HTGRS6008_A_B12-Opn5-ampicillin). The ES cells harbour a genetic modification wherein a *Lacz-Neomycin* cassette is flanked by FRT sites, between exon 3 and exon 4 and a *loxp* site separates *Lacz* from the neomycin coding region (Supplementary Fig. 1). *Loxp* sites also flank exon 4 of *Opn5* allowing multiple mouse lines that can serve as reporter

nulls, conditional floxed and null mice. The *Opn5*^{fl} allele was created by crossing the *Opn5*$^{tm1a(KOMP)Wtsi}$ mice to *FLPeR* (Jax stock #003946) to remove the *LacZ* cassette. The *Opn5*$^{-/-}$ line was created by crossing the *Opn5*^{fl} mice to *E2a-Cre* (Jax stock # 003724). Littermate control animals were used for all experiments with the exception of C57BL/6J mice reared under different lighting conditions.

The genotyping primers and protocol for alleles except *Opn5* are described in the cited publication or on the Jackson Labs website. Primer sequences for genotyping the *Opn5*$^{-/-}$ or *Opn5*$^{fl/fl}$ alleles are: F1: CACAGTATGTGTGACAACCT; R1: GTGGACAGATTAACTGAAGC; R2: GAACTGATGGCGAGCTCAGA. F1-R1 gives a 626 bp wild-type band and also gives a 700 bp band from the *Opn5*^{fl} allele. F1-R2 gives a 376 bp for *Opn5*^{null} and a 1617 bp band from the *Opn5*^{fl} allele. Primer sequences for genotyping the *Opn5*^{cre} allele are: Opn5creF1: TGGAAAGAGATGCATTTGTGAG; Opn5creF2: CACTGCATTCTAGTTGTGGTTTGTCC; Opn5creR1: ACAGCCTATGAATTCTCTCAATGC. F1R1 gives a 300 bp band for wild-type and F2R1 gives a 209 bp band for Cre allele.

The *Opn5*^{cre} was generated in-house using CRISPR-Cas9 technology. Four gRNAs that target exon 1 of *Opn5* were selected to knock in the Cre cassette. Plasmids containing the gRNA sequence were transfected into MK4 cells (an in-house mouse cell line representing induced metanephric mesenchyme undergoing epithelial conversion). The editing efficiency of gRNA was determined by T7E1 assay of PCR products of the target region amplified from genomic DNA of transfected MK4 cells. The sequence of the gRNA that was subsequently used for the transfection is TGGAGTCCTACTCGCGGACG. Sanger sequencing was performed to validate the knock-in sequence of founder mice.

Mice were placed on normal chow diet (NCD: 29% Protein, 13% Fat and 58% Carbohydrate kcal; LAB Diet #5010) ad libitum with free access to water. Littermate controls were used for genetic crosses and both male and female pups were included in the study.

Lighting conditions

Animals were housed in standard fluorescent lighting (photon flux 1.62×10^{15} photons/cm^2/sec) on a 12L:12D cycle except where noted. For full spectrum lighting (VBGR), LEDs were used to yield a comparable total photon flux of 1.68×10^{15} photons/cm^2/sec. Spectral and photon flux information for LED lighting: violet (λ_{max}=380 nm, 4.23×10^{14} photons/cm^2/sec in 370–400 nm range), blue (λ_{max}=480 nm, 5.36×10^{15} photons/cm^2/sec in 430–530 nm range), green (λ_{max}=530 nm, 5.82×10^{15} photons/cm^2/sec in 480–600 nm range) and red (λ_{max}=630 nm, 1.93×10^{15} photons/cm^2/sec in 590–660 nm range). For wavelength restricted hyaloid assessment, C57BL/6J animals were housed in 12L:12D cycle starting late gestation (embryonic day E18) either in full spectrum (VBGR) or without violet (BGR) lighting. For dark-reared (DD) experiments, pregnant dams were moved to dark at gestation age E16. For light induction experiments, on P7 at lights off, nursing females and pups were moved to DD for 24-hour dark-adaptation. *Opn5*$^{+/+}$ and *Opn5*$^{-/-}$ pups were subjected to ±30 minutes of 380 nm light at 1×10^{12} photons/cm^2/sec (approximately 1% of clear sky summer day sunlight at this wavelength) at two hours after subjective lights off.

Immunohistochemistry and imaging

Animals were anaesthetized under isoflurane and sacrificed by cervical dislocation or decapitation for early post-natal pups. Preparation and immunofluorescence staining of retinae and hyaloid vessels were as described previously[6]. For phospho-T53-DAT (pDAT) quantification, retinae of each genotype and light condition were collected in dim red light (dark-adapted) or normal light from at least 3 different induction experiments and mounted in the same OCT blocks. Retinal sections were processed, stained, and imaged together to compensate for batch differences. Alexa-conjugated secondary antibodies were purchased from Jackson ImmunoResearch (JIR). Images were captured using Zeiss ApoTome AX10 or Zeiss LSM700 confocal microscopes and processed by ImageJ (NIH) and Adobe Photoshop (Adobe Systems). Primary antibodies and lectins used in this study are listed in Supplementary Table 1.

ELISA

Vitreous and retinae from pups were collected and rapidly frozen on dry ice. To detect dopamine levels, vitreal samples were pooled from 3–6 pups depending on age and 6 retinae for each “n”. Dopamine extraction and ELISA assay were performed according to manufacture protocol using BA E-5300 (Rocky Mountain Diagnostics). For DD experiments, vitreous and retinae were collected under dim red light. To detect VEGFA and FLT1 levels, samples from P5 pups were pooled from 6 eyes for each “n”. Mouse VEGFA kit, Quantikine (MMV00) and mouse VEGFR1 (FLT1), Quantikine (MVR100) from R&D systems were used. ELISA was read by using EnVision Multimode Plate Reader (Perkin Elmer).

Pharmacological reagents and treatments

All dopamine pharmacological modulators, except for antagonists 2-CMDO (2-Chloro-11-(4-methylpiperazino)dibenz(*Z*)[*b,f*]oxepin maleate), were injected at 1 mg/kg body weight[7] intraperitoneally (i.p.) into nursing dams on day of birth and P2, then directly into pups until P8. 2-CMDO was injected into pups P5-P8 at 2 mg/kg body weight. Injection was done in dim red light one hour before lights on. Dopamine agonist SKF38393 hydrobromide; high affinity D_2 antagonist L-741626; dopamine transporter 1 inhibitor, GBR12909 dihydrochloride; 2-CMDO were all purchased from Tocris Biosciences. For experiments with *Pdgfb-icreERT2* mouse lines, 2 mg Tamoxifen was injected into nursing dams on the day of birth and on P2 to activate tamoxifen-dependent cre.

Western Blotting

Western blots were performed using standard protocols. Immediately after dissection, twelve hyaloid vascular tissues or retinae of P6 (six pups) were pooled in 100 μl of 1x Laemmli sample buffer and sonicated. After centrifugation, 20 μl of supernatant was loaded on 4 to 20% gradient protein gel (ThermoFisher Scientific). Separated protein bands were transferred to PVDF membrane, and bands were visualized by chemiluminescence (ThermoFisher Scientific). Unprocessed immunoblots are available in Supplementary Fig. 6. Band intensity was measured by ImageJ (NIH). Following antibodies were used for Western blotting: VEGFR2 (Cell Signaling Technology, #9698), phospho-VEGFR2 (Cell Signaling

Technology, #2478), β-tubulin (Abcam, ab6046), DAT (Novus, NB300–254), phospho-DAT (ThermoFisher Scientific, PA5–35414), AKT (Cell Signaling Technology, #4691) and phospho-AKT S473 (Cell Signaling Technology, #4060). All antibodies were used at 1:1000 dilution.

Statistics and Reproducibility

Samples for immunoblots were pooled from multiple animals (six pups for hyaloid vasculature and six retinae) and each experiment repeated at least twice with independent samples. Unprocessed western blots are available in Supplementary Fig. 6. ELISA assessment was performed at least twice with independent biological samples. Each n in this analysis is a separate animal with the exception that for immunoblots and ELISA, pooled samples from animals of the same genotype represent one n. Retinal images with immunofluorescence labelling represent n=3 independent biological samples from separate litters. Data gathered for hyaloid vessel quantification represents samples from multiple litters to reach n indicated on charts for each genotype and condition. Data are presented as mean±s.e.m in aligned dot plots overlaid with bar or line graph. Statistical analyses were performed using GraphPad Prism version 4.00 (GraphPad Software) and Microsoft Excel for Two Tailed Student's T-test, One-way or Two-way ANOVA as indicated. Two-tailed distribution, two-sample unequal variance *t*-test was used to determine the statistical significance between two independent groups except for Fig. 6m which is one-tailed. Sidak's or Tukey's multiple comparison test were performed post-hoc when significance differences were found in ANOVA.

Data availability

Source data for all figures have been provided as Supplementary Table 2.

Additional experimental repeats for key retinal labelling experiments have been deposited on Figshare (doi:10.6084/m9.figshare.7450961).

All other data supporting the findings of this study are available from the corresponding author on reasonable request.

Supplementary Material

Refer to Web version on PubMed Central for supplementary material.

Acknowledgements

We thank (1) Paul Speeg (Lang lab) for excellent mouse colony management, (2) Leela Sankaran and Polina Lyuboslavsky (Iuvone lab) for technical assistance, and (3) Derek Bredl and David Copenhagen (UCSF) for providing tissue samples from the *Drd2-eGFP* mice. We would also like to thank Yinhuai Chen and Yueh-Chiang Hu of the CCHMC Transgenic Animal and Genome Editing Core Facility for generating genetically modified mouse lines. This work was supported by NIH R01 GM124246 to EDB, NIH R01EY026921 to RVG, NIH P30EY001730 to University of Washington, the Mark J. Daily, MD Research Fund to University of Washington, and unrestricted grants to the University of Washington and Emory University Departments of Ophthalmology from Research to Prevent Blindness. This work was also supported by NIH grants R01 EY027077 (Lang and Rao), R01 EY027711 (Iuvone and Lang), R01 EY022917 (Hegde), R01 EY004864 (PMI), by funds from the Goldman Chair of the Abrahamson Pediatric Eye Institute at Cincinnati Children's Hospital Medical Center and by grant BIOCEV-CZ.1.05/1.1.00/02.0109 (Kozmik). This work was supported by NIH Grant 2T32GM063483, which supports the UCCOM/CCHMC Medical Scientist Training Program.

References

1. Schiller PH & Tehovnik EJ Vision and the Visual System. (Oxford University Press, 2015).
2. Bass J & Takahashi JS Circadian integration of metabolism and energetics. Science 330, 1349–54 (2010). [PubMed: 21127246]
3. Partch CL, Green CB & Takahashi JS Molecular architecture of the mammalian circadian clock. Trends Cell Biol 24, 90–99 (2014). [PubMed: 23916625]
4. Terakita A & Nagata T Functional Properties of Opsins and their Contribution to Light-Sensing Physiology. Zoolog. Sci 31, 653–659 (2014). [PubMed: 25284384]
5. Shichida Y & Matsuyama T Evolution of opsins and phototransduction. Philos. Trans. R. Soc. B Biol. Sci 364, 2881–2895 (2009).
6. Nathans J Rhodopsin: structure, function, and genetics. Biochemistry 31, 4923–31 (1992). [PubMed: 1599916]
7. Palczewski K & Orban T From Atomic Structures to Neuronal Functions of G Protein–Coupled Receptors. Annu. Rev. Neurosci 36, 139–164 (2013). [PubMed: 23682660]
8. Provencio I, Rollag MD & Castrucci AM Photoreceptive net in the mammalian retina. This mesh of cells may explain how some blind mice can still tell day from night. Nature 415, 493 (2002).
9. Hattar S, Liao HW, Takao M, Berson DM & Yau KW Melanopsin-containing retinal ganglion cells: architecture, projections, and intrinsic photosensitivity. Science (80-.). 295, 1065–1070 (2002).
10. Berson DM, Dunn FA & Takao M Phototransduction By Retinal Ganglion Cells That Set The Circadian Clock. Science (80-.). 295, 1070–1073 (2002).
11. Yamashita T et al. Evolution of mammalian Opn5 as a specialized UV-absorbing pigment by a single amino acid mutation. J Biol Chem 289, 3991–4000 (2014). [PubMed: 24403072]
12. Sato K et al. Two UV-sensitive photoreceptor proteins, Opn5m and Opn5m2 in ray-finned fish with distinct molecular properties and broad distribution in the retina and brain. PLoS One 11, (2016).
13. Yamashita T et al. Opn5 is a UV-sensitive bistable pigment that couples with Gi subtype of G protein. Proc Natl Acad Sci U S A 107, 22084–22089 (2010). [PubMed: 21135214]
14. Kojima D et al. UV-sensitive photoreceptor protein OPN5 in humans and mice. PLoS One 6, e26388 (2011). [PubMed: 22043319]
15. Tarttelin EE, Bellingham J, Hankins MW, Foster RG & Lucas RJ Neuropsin (Opn5): a novel opsin identified in mammalian neural tissue. FEBS Lett 554, 410–416 (2003). [PubMed: 14623103]
16. Nakane Y et al. A mammalian neural tissue opsin (Opsin 5) is a deep brain photoreceptor in birds. Proc. Natl. Acad. Sci 107, 15264–15268 (2010). [PubMed: 20679218]
17. Ota W, Nakane Y, Hattar S & Yoshimura T Impaired Circadian Photoentrainment in Opn5-Null Mice. iScience 6, 299–305 (2018). [PubMed: 30240620]
18. Buhr ED et al. Neuropsin (OPN5)-mediated photoentrainment of local circadian oscillators in mammalian retina and cornea. Proc. Natl. Acad. Sci. U. S. A 112, (2015).
19. Joyner AL & Zervas M Genetic inducible fate mapping in mouse: establishing genetic lineages and defining genetic neuroanatomy in the nervous system. Dev. Dyn 235, 2376–85 (2006). [PubMed: 16871622]
20. Cai D, Cohen KB, Luo T, Lichtman JW & Sanes JR Improved tools for the Brainbow toolbox. Nat. Methods 10, 540–547 (2013).
21. Rodriguez AR, de Sevilla Muller LP & Brecha NC The RNA binding protein RBPMS is a selective marker of ganglion cells in the mammalian retina. J Comp Neurol 522, 1411–1443 (2014). [PubMed: 24318667]
22. Frielingsdorf H et al. Variant brain-derived neurotrophic factor Val66Met endophenotypes: implications for posttraumatic stress disorder. Ann N Y Acad Sci 1208, 150–157
23. Rao S et al. A direct and melanopsin-dependent fetal light response regulates mouse eye development. Nature 494, 243–246 (2013). [PubMed: 23334418]
24. Lobov IBB et al. WNT7b mediates macrophage-induced programmed cell death in patterning of the vasculature. Nature 437, 417–421 (2005). [PubMed: 16163358]
25. Ferrara N Vascular endothelial growth factor: basic science and clinical progress. Endocr Rev 25, 581–611 (2004). [PubMed: 15294883]

26. Dickson PW & Briggs GD Tyrosine hydroxylase. Regulation by feedback inhibition and phosphorylation. Adv. Pharmacol 68, 13–21 (2013). [PubMed: 24054138]
27. Basu S et al. The neurotransmitter dopamine inhibits angiogenesis induced by vascular permeability factor/vascular endothelial growth factor. Nat. Med 7, 569–574 (2001). [PubMed: 11329058]
28. Sinha S et al. Dopamine regulates phosphorylation of VEGF receptor 2 by engaging Src-homology-2-domain-containing protein tyrosine phosphatase 2. J Cell Sci 122, 3385–3392 (2009). [PubMed: 19706677]
29. Wulle I & Schnitzer J Distribution and morphology of tyrosine hydroxylase-immunoreactive neurons in the developing mouse retina. Brain Res Dev Brain Res 48, 59–72 (1989). [PubMed: 2568894]
30. Witkovsky P, Nicholson C, Rice ME, Bohmaker K & Meller E Extracellular dopamine concentration in the retina of the clawed frog, Xenopus laevis. Proc. Natl. Acad. Sci. U. S. A 90, 5667–71 (1993). [PubMed: 8516316]
31. Newkirk GS, Hoon M, Wong RO & Detwiler PB Inhibitory inputs tune the light response properties of dopaminergic amacrine cells in mouse retina. J. Neurophysiol 110, 536–552 (2013). [PubMed: 23636722]
32. Cameron MA et al. Light regulation of retinal dopamine that is independent of melanopsin phototransduction. Eur J Neurosci 29, 761–767 (2009). [PubMed: 19200071]
33. Iuvone PM, Galli CL, Garrison-Gund CK & Neff NH Light stimulates tyrosine hydroxylase activity and dopamine synthesis in retinal amacrine neurons. Science (80-.). 202, 901–902 (1978).
34. Witkovsky P, Gabriel R, Haycock JW & Meller E Influence of light and neural circuitry on tyrosine hydroxylase phosphorylation in the rat retina. J Chem Neuroanat 19, 105–116 (2000). [PubMed: 10936746]
35. Jackson CR, Capozzi M, Dai H & McMahon DG Circadian Perinatal Photoperiod Has Enduring Effects on Retinal Dopamine and Visual Function. J. Neurosci 34, 4627–4633 (2014). [PubMed: 24672008]
36. Vaughan RA & Foster JD Mechanisms of dopamine transporter regulation in normal and disease states. Trends in Pharmacological Sciences 34, 489–496 (2013). [PubMed: 23968642]
37. Foster JD et al. Dopamine transporter phosphorylation site threonine 53 regulates substrate reuptake and amphetamine-stimulated efflux. J. Biol. Chem 287, 29702–29712 (2012). [PubMed: 22722938]
38. Rothman RB et al. GBR12909 antagonizes the ability of cocaine to elevate extracellular levels of dopamine. Pharmacol. Biochem. Behav 40, 387–397 (1991). [PubMed: 1839568]
39. Rao S et al. A direct and melanopsin-dependent fetal light response regulates mouse eye development. Nature 494, (2013).
40. Benoit-Marand M, Ballion B, Borrelli E, Boraud T & Gonon F Inhibition of dopamine uptake by D2 antagonists: An in vivo study. J. Neurochem 116, 449–458 (2011). [PubMed: 21128941]
41. Hack I, Peichl L & Brandstätter JH An alternative pathway for rod signals in the rodent retina: rod photoreceptors, cone bipolar cells, and the localization of glutamate receptors. Proc. Natl. Acad. Sci. U. S. A 96, 14130–5 (1999). [PubMed: 10570210]
42. YANG X Characterization of receptors for glutamate and GABA in retinal neurons. Prog. Neurobiol 73, 127–150 (2004). [PubMed: 15201037]
43. Delwig A et al. Glutamatergic neurotransmission from melanopsin retinal ganglion cells is required for neonatal photoaversion but not adult pupillary light reflex. PLoS One 8, e83974 (2013). [PubMed: 24391855]
44. Johnson J et al. Vesicular neurotransmitter transporter expression in developing postnatal rodent retina: GABA and glycine precede glutamate. J Neurosci 23, 518–529 (2003). [PubMed: 12533612]
45. Hirano AA et al. Targeted Deletion of Vesicular GABA Transporter from Retinal Horizontal Cells Eliminates Feedback Modulation of Photoreceptor Calcium Channels. eneuro 3, ENEURO.0148–15.2016 (2016).
46. Johnson J et al. Vesicular glutamate transporter 1 is required for photoreceptor synaptic signaling but not for intrinsic visual functions. J Neurosci 27, 7245–7255 (2007). [PubMed: 17611277]

47. Rowan S & Cepko CL Genetic analysis of the homeodomain transcription factor Chx10 in the retina using a novel multifunctional BAC transgenic mouse reporter. Dev. Biol 271, 388–402 (2004). [PubMed: 15223342]
48. Jackson CR et al. Retinal dopamine mediates multiple dimensions of light-adapted vision. J Neurosci 32, 9359–9368 (2012). [PubMed: 22764243]
49. Klimova L, Lachova J, Machon O, Sedlacek R & Kozmik Z Generation of mRx-Cre transgenic mouse line for efficient conditional gene deletion in early retinal progenitors. PLoS One 8, e63029 (2013). [PubMed: 23667567]
50. Setler PE, Sarau HM, Zirkle CL & Saunders HL The central effects of a novel dopamine agonist. Eur J Pharmacol 50, 419–430 (1978). [PubMed: 568069]
51. Bhattacharya R et al. The neurotransmitter dopamine modulates vascular permeability in the endothelium. J Mol Signal 3, 14 (2008). [PubMed: 18662404]
52. Shatz CJ Emergence of order in visual system development. in Journal of Physiology Paris 90, 141–150 (1996).
53. Wong ROL RETINAL WAVES AND VISUAL SYSTEM DEVELOPMENT. Annu. Rev. Neurosci 22, 29–47 (1999). [PubMed: 10202531]
54. Arroyo DA, Kirkby LA & Feller MB Retinal Waves Modulate an Intraretinal Circuit of Intrinsically Photosensitive Retinal Ganglion Cells. J. Neurosci 36, 6892–6905 (2016). [PubMed: 27358448]
55. Hussein MA et al. Evaluating the association of autonomic drug use to the development and severity of retinopathy of prematurity. J AAPOS 18, 332–337 (2014). [PubMed: 25173894]
56. Michael Iuvone P Is retinal dopamine involved in the loss of visual function in retinopathy of prematurity? Investigative Ophthalmology and Visual Science 57, 3380 (2016). [PubMed: 27367505]
57. Yang MBB, Rao S, Copenhagen DRR & Lang RAA Length of day during early gestation as a predictor of risk for severe retinopathy of prematurity. Ophthalmology 120, 2706–2713 (2013). [PubMed: 24139125]
58. Torii H et al. Violet Light Exposure Can Be a Preventive Strategy Against Myopia Progression. EBioMedicine 15, 210–219 (2017). [PubMed: 28063778]
59. Zhou X, Pardue MT, Iuvone PM & Qu J Dopamine signaling and myopia development: What are the key challenges. Progress in Retinal and Eye Research 61, 60–71 (2017). [PubMed: 28602573]
60. Claxton S et al. Efficient, inducible Cre-recombinase activation in vascular endothelium. Genesis 46, 74–80 (2008). [PubMed: 18257043]
61. Nelson AB et al. A Comparison of Striatal-Dependent Behaviors in Wild-Type and Hemizygous Drd1a and Drd2 BAC Transgenic Mice. J. Neurosci 32, 9119–9123 (2012). [PubMed: 22764221]
62. Panda S et al. Melanopsin is required for non-image-forming photic responses in blind mice. Science (80-.). 301, 525–527 (2003).

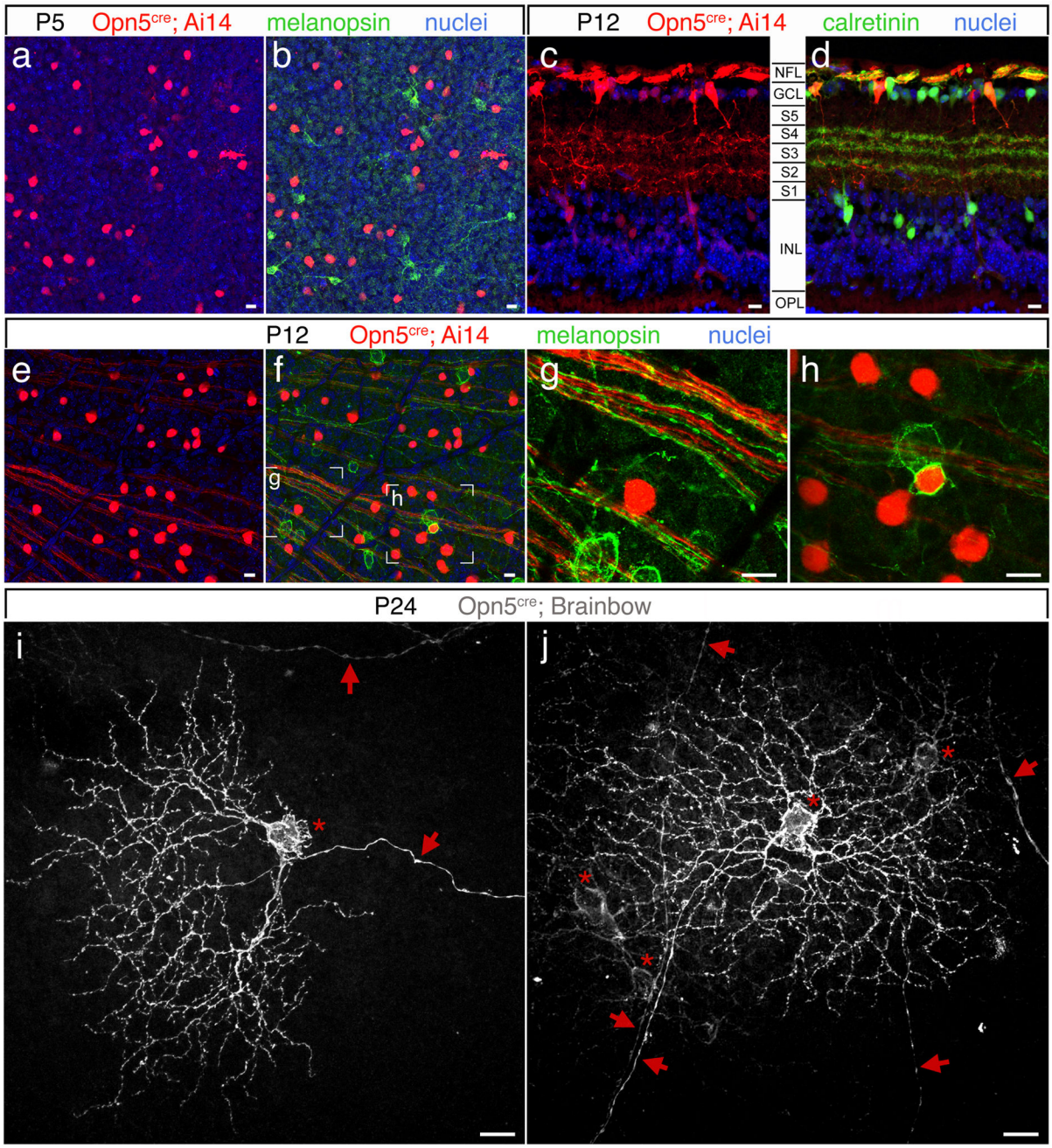

Figure 1. *Opn5* is expressed in a distinct subset of retinal ganglion cells.

a, **b**, Flat mount retina from P5, *Opn5*^{cre}*; Ai14* mice showing the tdTomato cre reporter (**a**, **b**, red), nuclear labelling with Hoechst 33258 (**b**, blue), and counter labelling for melanopsin (**b**, green). **c**, **d**, Retinal cryosections from P12, *Opn5*^{cre}*; Ai14* mice showing the tdTomato cre reporter (**c**, **d**, red), nuclei with Hoechst 33258 (**c**, **d**, blue), and labeling for calretinin (**c**, green). Retinal laminae are indicated by the abbreviation between the panels: NFL; nerve fibre layer, GCL: ganglion cell layer; S5-S1; sublaminae of the inner plexiform layer, INL: inner nuclear layer, OPL: outer plexiform layer. **e-h**, As in (**a, b**) except at P12. **g**, **h**, show magnified regions of (**e**) as indicated by white corner marks. **i**, **j**, Flat mount retinae showing

labelling of cell bodies (asterisks), dendritic fields and axons (arrows) for retinal ganglion cells labelled by the *Brainbow3.2* reporter in P24 *Opn5*^{cre} mice. Scale bars are 20 μm. Panels a-j are representative of at least 3 separate experiments. Additional examples of these images are available on Figshare.

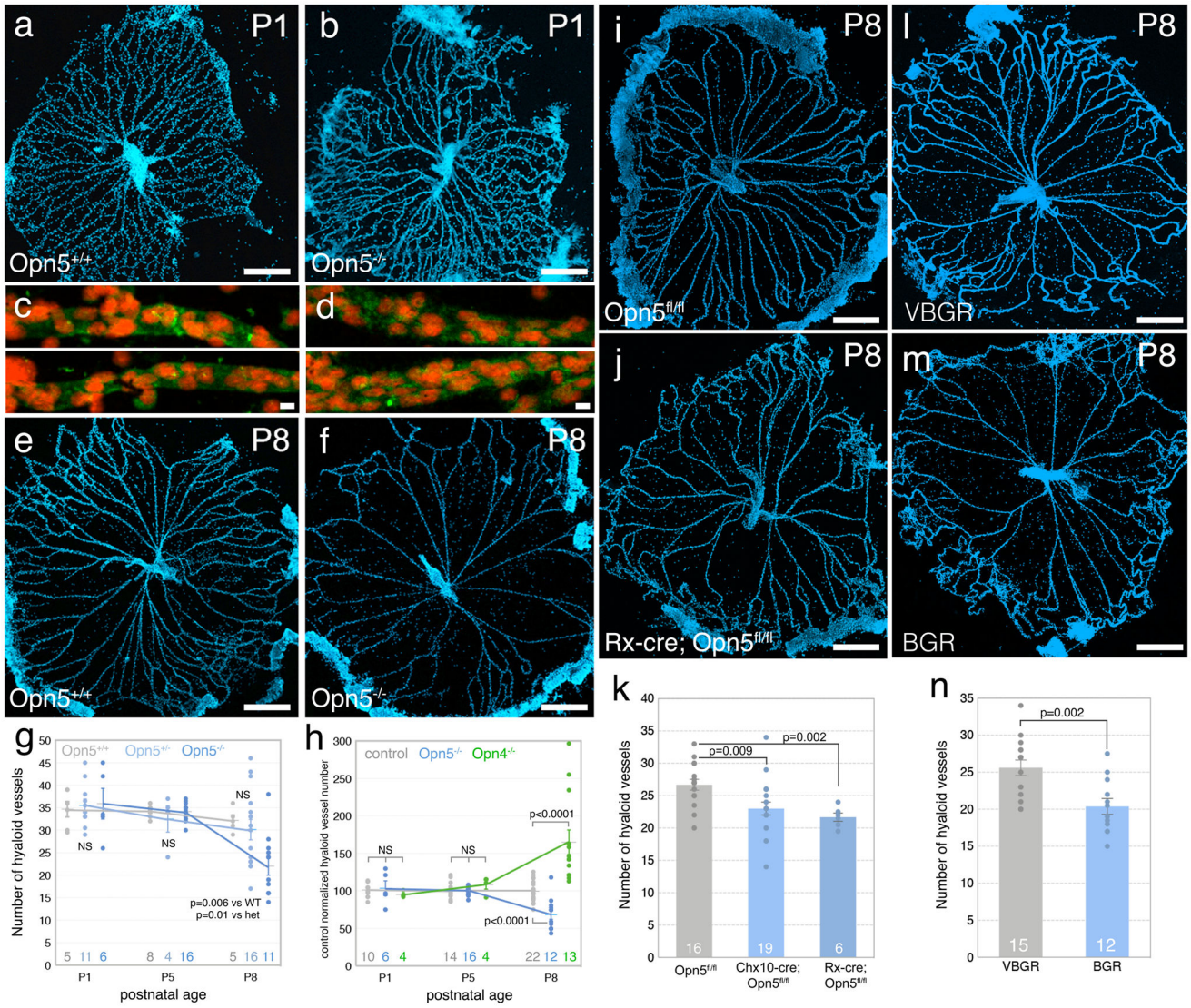

Figure 2. Precocious hyaloid vessel regression in the *Opn5* null and absence of 380 nm photons.

a, b, Hoechst 33258 (blue) labelled hyaloid vessel preparations from P1 *Opn5*$^{+/+}$ and *Opn5*$^{-/-}$ mice. **c, d,** Higher magnification images of two examples each of P1 hyaloid vessel segments from *Opn5*$^{+/+}$ (**c**) and *Opn5*$^{-/-}$ (**d**) mice labelled with Hoechst 33258 (presented in red) and isolectin (green). **e, f**, Hoechst 33258 labelled hyaloid vessel preparations from P8 *Opn5*$^{+/+}$ and *Opn5*$^{-/-}$ mice. **g**, Quantification of hyaloid vessel number in *Opn5*$^{+/+}$ (grey), *Opn5*$^{+/-}$ (light blue) and *Opn5*$^{-/-}$ (dark blue) mice over a P1-P8 time-course. **h**, as in (e) but relative hyaloid vessel numbers for control (grey), *Opn5*$^{-/-}$ (blue), and *Opn4*$^{-/-}$ (green) mice. **i, j**, Hoechst 33258 labelled hyaloid vessel preparations from P8 *Opn5*$^{fl/fl}$ control and *Opn5*$^{fl/fl}$; *Rx-cre* mice. **k**, Quantification of P8 hyaloid vessel number in *Opn5*$^{fl/fl}$ control (grey), *Opn5*$^{fl/fl}$; *Chx10-cre* (light blue), and *Opn5*$^{fl/fl}$; *Rx-cre* (dark blue) mice. **l, m,** Hoechst 33258 labelled hyaloid vessel preparations from P8 mice raised from birth in full spectrum (V, violet + B, blue, + G, green, + R, red) or "minus violet" (BGR) lighting. **n,** Quantification of P8 hyaloid vessel number from P8 mice raised from birth in full spectrum

(grey bar) or “minus violet” (blue bar) lighting. All p-values by Student T-test. The number at the base of each chart is n and represents the number of animals assessed. Error bars are SEM. Scale bars 400 μm (a,b,e,f,I,j,l,m) 20 μm (c,d).

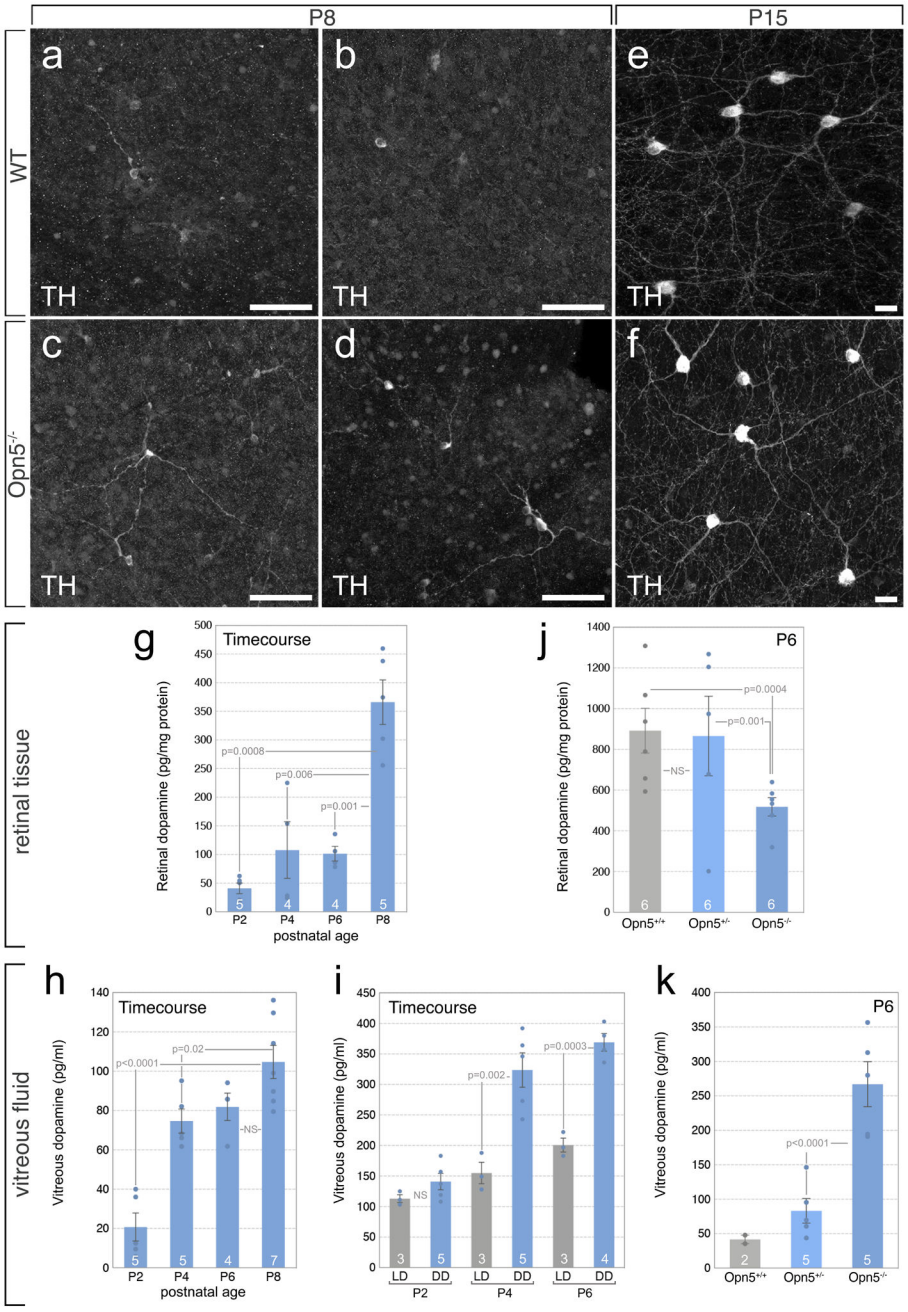

Figure 3. OPN5- and light-dependent pathways regulate dopamine levels in the neonatal mouse eye.

a-f, Immunofluorescent labelling for tyrosine hydroxylase (TH, greyscale) in flat mount retinae from control *Opn5*$^{+/+}$ (**a, b, e**) and *Opn5*$^{-/-}$ (**c, d, f**) mice at P8 (**a-d**) and P15 (**e, f**). Scale bars 100 μm (a-d) 20 μm (e,f). **g-k**, Charts showing ELISA quantification of dopamine in retinal lysates (**g, j**) and vitreous fluid (**h, i k**). **g, h,** Dopamine levels in each tissue over a P2-P8 developmental time-course. **i,** Dopamine levels over a P2-P6 developmental time course comparing normal lighting (LD) with the consequences of dark rearing (DD). **j, k**, Dopamine levels in retinal lysate (**j**) and vitreous fluid (**k**) from P6 *Opn5*$^{+/+}$ control (**j, k,**

grey bars), *Opn5*$^{+/-}$ heterozygote (**j, k,** light blue bars), and *Opn5*$^{-/-}$ homozygote (**j, k,** light blue bars). p-values by (**g, h**) Two Way ANOVA, (**i**) Student's T-test, (**j, k**) One Way ANOVA. Error bars are SEM. The number at the base of each chart is n and represents the number of animals assessed. Panels a-f are representative of at least 3 separate experiments. Additional examples of (**a-d**) are available on Figshare.

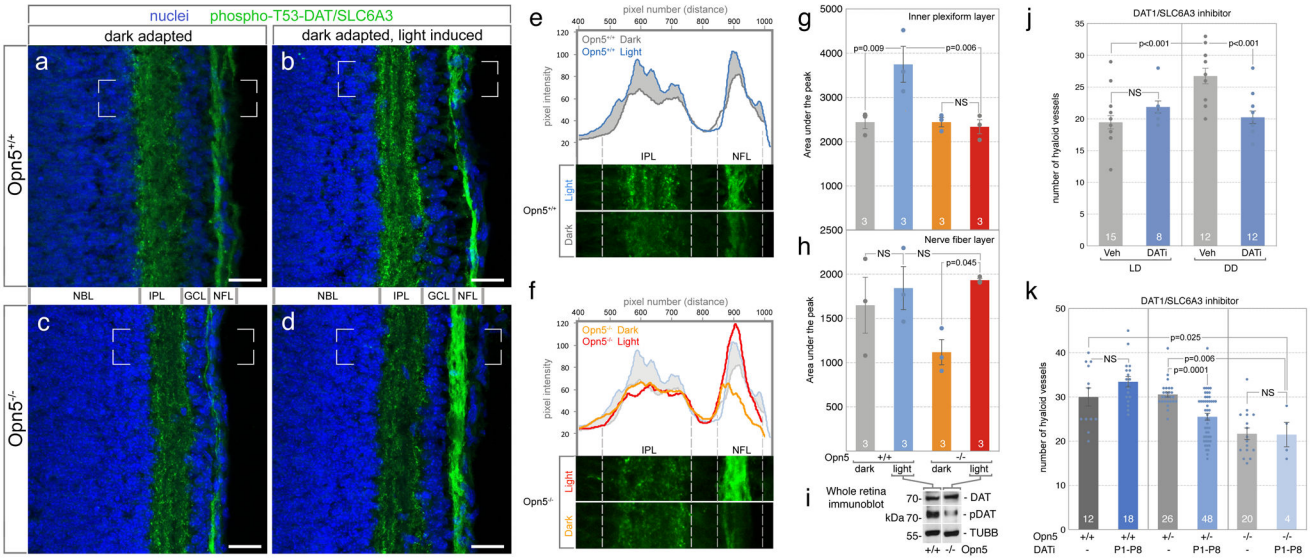

Figure 4. Light-dependent activation of phospho-T53-DAT/SLC6A3 in the IPL requires OPN5.

a, **b**, Labelling of P8 *Opn5*$^{+/+}$ retina for nuclei (blue) and phospho-T53-DAT (green) for dark adapted mice half of which were exposed to 30 minutes of 380 nm light. NBL: neuroblastic layer. IPL: inner plexiform layer. GCL: ganglion cell layer. NFL: nerve fibre layer. Scale bars 50 μm. Indicated areas of each panel are exported to chart (**e**). **e**, Chart showing averaged (n=3) quantification profiles (dark adapted, grey trace, light exposed, blue trace) for phospho-T53-DAT in retinal cryosections (**a, b**). Grey shading emphasizes the elevated signal of light-induced sample. **c, d**, As in (**a, b**) but for *Opn5*$^{-/-}$ retina. **f**, Chart as in (e) except for *Opn5*$^{-/-}$ mice (dark-adapted, orange trace, or dark adapted and exposed to 380 nm light for 30 minutes, red trace). Traces from chart (**e**) are reproduced on chart (**f**) for comparison. **g, h**, Charts showing under-the-peak quantification (n=3) of phospho-T53-DAT labelling in inner plexiform layer (**g**) and nerve fibre layer (**h**) for P8 mice of the labelled genotype and light exposure. The vertical dashed lines in (**e, f**) indicate the areas that were quantified. **i,** Immunoblot detecting DAT/SLC6A3 (DAT), phospho-T53-DAT/SLC6A3 (pDAT) and β-tubulin (TUBB) in retinae harvested from *Opn5*$^{+/+}$ (left lane) and *Opn5*$^{-/-}$ (right lane) mice during the light phase. phospho-T53-DAT/SLC6A3 is lower than normal in the *Opn5* null. Unprocessed blot image in Supplementary Figure 6. **j**, Quantification of P8 hyaloid vessels in WT mice injected with vehicle or with the DAT/SLC6A3 inhibitor raised from E17 either in normal (LD) lighting, or in constant darkness (DD). **k**, Quantification of P8 hyaloid vessels in *Opn5*$^{+/+}$, *Opn5*$^{+/-}$, and *Opn5*$^{-/-}$ mice injected from P1-P8 with the DAT/SLC6A3 inhibitor. p-values by Two Way ANOVA. Error bars are SEM. The number at the base of each chart is n and represents the number of animals assessed. Panels a-d are representative of 3 separate experiments.

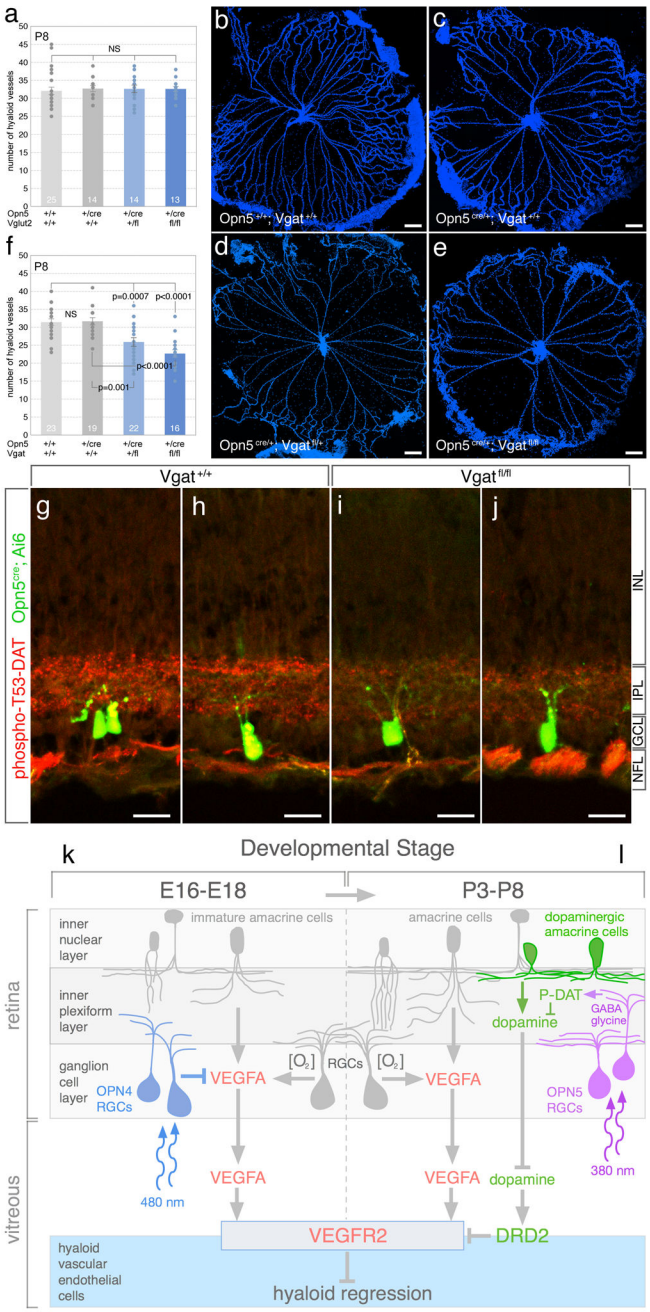

Figure 5. OPN5 RGCs use *Vgat* in a hyaloid regression pathway: A model for OPN4-VEGFA and OPN5-dopamine pathway integration.

a, Quantification of hyaloid vessels in P8 *Opn5*$^{+/+}$; *Vglut2*$^{+/+}$ (light grey), *Opn5*$^{+/cre}$; *Vglut2*$^{+/+}$ (dark grey), *Opn5*$^{+/cre}$; *Vglut2*$^{fl/+}$ (light blue), *Opn5*$^{+/cre}$; *Vglut2*$^{fl/fl}$ (dark blue) mice. **b-e,** Hyaloids from P8 *Opn5*$^{+/+}$; *Vgat*$^{+/+}$ (**b**), *Opn5*$^{+/cre}$; *Vgat*$^{+/+}$ (**c**), *Opn5*$^{+/cre}$; *Vgat*$^{fl/+}$ (**d**), *Opn5*$^{+/cre}$; *Vgat*$^{fl/fl}$ (**e**) mice. **f**, Quantification of hyaloid vessels in P8 mice with genotypes listed in **b-e**. **g-h**, Retinal cryosections imaged for phospho-T53-DAT (red) and *Ai6* cre (green) from P8 *Ai6*; *Opn5*^{cre}; *Vgat*$^{+/+}$ (**g,h**) or *Ai6*; *Opn5*^{cre}; *Vgat*$^{fl/fl}$ (**i, j**) mice. Additional examples of (**g-j**) available on Figshare. Sample size (n) for a,f is shown at

the base of each bar and represents mice. p values by one-way ANOVA. Error bars are SEM. Images in b-e represent at least six, and in g-j at least three, separate experiments. Scale bars 200 μm (b-e) 20 μm (g-j). **k**, **l,** Schematic describing integration of the OPN4-VEGFA and OPN5-dopamine hyaloid regression pathways. The schematic identifies two phases of development, E16-E18 (**k**), and P3-P8 (**l**), when OPN4 and OPN5 are each required. In late gestation, blue light stimulation of OPN4 RGCs suppresses retinal cellularity. In dark-reared or in *Opn4* null mice, elevated cellularity increases oxygen demand ($[O_2]$) and, *via* the hypoxia response pathway, increases VEGFA expression in amacrine cells and RGCs. Elevated VEGFA causes promiscuous retinal angiogenesis and suppresses hyaloid vessel regression. According to the present analysis, violet light stimulation of OPN5 RGCs postnatally suppresses dopamine in the vitreous by upregulating T53 phosphorylation of the dopamine transporter (P-DAT/SLC6A3) in neurons in the inner plexiform layer. Normally, OPN5-dependent phosphorylation of DAT results in elevated dopamine uptake and a reduced flux of dopamine from dopaminergic amacrine cells to the vitreous. In the absence of OPN5, or the violet light that stimulates OPN5, vitreous dopamine is precociously elevated. This results in premature activation of dopamine receptor DRD2 in hyaloid VECs, suppression of VEGFR2 survival signalling and precocious regression. These data indicate that both 480 nm blue light *via* OPN4, and 380 nm violet light *via* OPN5, function as developmental timing cues.

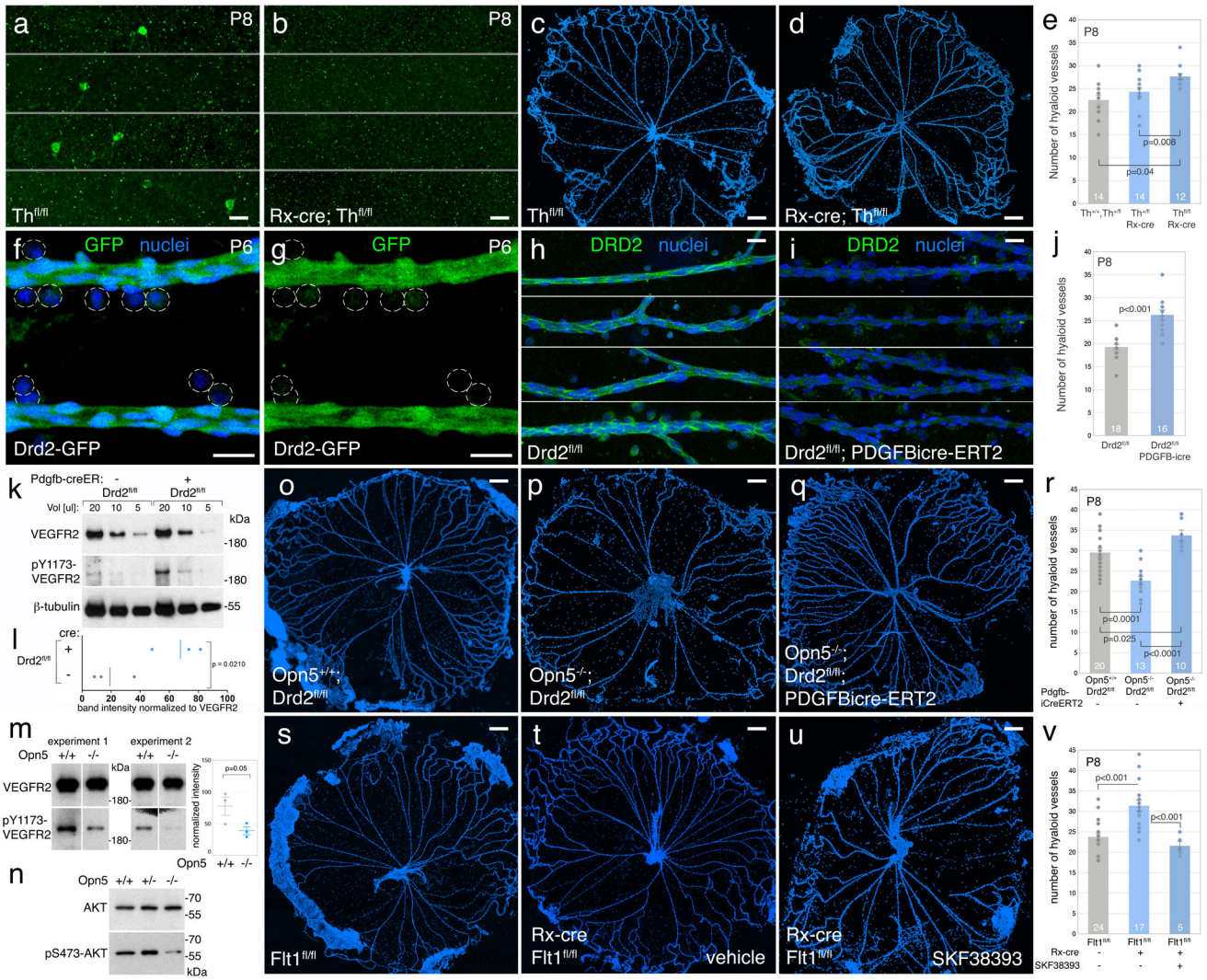

Figure 6. Retinal dopamine promotes hyaloid vessel regression via DRD2-dependent suppression of VEGFR2 activity.

a, **b**, TH labelling (green) in four regions of P8 flat mount retinae from *Th*$^{fl/fl}$ (**a**) and *Rx-cre; Th*$^{fl/fl}$ (**b**) mice. **c, d,** Hyaloids from P8 control *Th*$^{fl/fl}$ (**c**) and *Rx-cre; Th*$^{fl/fl}$ (**d**) mice. **e**, P8 hyaloid vessel numbers in control (*Th*$^{+/+}$ or *Th*$^{+/fl}$, grey), *Rx-cre; Th*$^{+/fl}$ (light blue), and *Rx-cre; Th*$^{fl/fl}$ (dark blue) mice. **f**, **g**, Hyaloid vessels from *Drd2-GFP* mice showing reporter expression (green) in vessels but not macrophages (circles). **h**, **i**, Immunolabelling for DRD2 in P8 hyaloids from tamoxifen treated *Drd2*$^{fl/fl}$ (**h**) and *Drd2*$^{fl/fl}$*; Pdgfb-icreERT2* (**i**) mice. **j**, P8 hyaloid vessel numbers in *Drd2*$^{fl/fl}$ (grey) and *Drd2*$^{fl/fl}$*; Pdgfb-icreERT2* (blue) mice. **k**, Immunoblots for VEGFR2, VEGFR2 pY1173, and β-tubulin in P6 hyaloid vessel lysates from *Drd2*$^{fl/fl}$ and *Drd2*$^{fl/fl}$*; Pdgfb-icreERT2* mice. Hyaloid lysate is loaded in successively halved volumes to ensure linear range detection. **l**, Band intensity of n=3 mice, pY1173 VEGFR2, normalized to total VEGFR2 from (**k**) confirms that in the *Drd2* mutant, active VEGFR2 is higher. **m, n,** Immunoblots for VEGFR2, pY1173-VEGFR2 (**m**), AKT and pS473-AKT (**n**) from P6 hyaloids of indicated genotypes. **m**, Quantification of pY1173-VEGFR2 relative to VEGFR2 in *Opn5*$^{+/+}$ (grey) and *Opn5*$^{-/-}$ (blue) hyaloid vessels.

pY1173-VEGFR2 and pS473-AKT levels are lower in *Opn5*$^{-/-}$. n=3 mice. Unprocessed blot images in Supplementary Figure 6. **o-q**, P8 hyaloids from tamoxifen treated *Opn5*$^{+/+}$; *Drd2*$^{fl/fl}$ (**o**), *Opn5*$^{-/-}$; *Drd2*$^{fl/fl}$ (**p**), and *Opn5*$^{-/-}$; *Drd2*$^{fl/fl}$*; Pdgfb-icreERT2* (**q**) mice. **r**, P8 hyaloid vessel numbers in *Opn5*$^{+/+}$; *Drd2*$^{fl/fl}$ (grey), *Opn5*$^{-/-}$; *Drd2*$^{fl/fl}$ (light blue), and *Opn5*$^{-/-}$; *Drd2*$^{fl/fl}$*; Pdgfb-icreERT2* (dark blue) mice. **s-u**, P8 hyaloid preparations from *Flt1*$^{fl/fl}$ (**s**), *Rx-cre*; *Flt1*$^{fl/fl}$ (**t**), and SKF38393 injected, *Rx-cre*; *Flt1*$^{fl/fl}$ (**u**) mice. **v**, P8 hyaloid vessel numbers in control *Flt1*$^{fl/fl}$ (grey), *Rx-cre*; *Flt1*$^{fl/fl}$ (light blue), and SKF38393 injected, *Rx-cre*; *Flt1*$^{fl/fl}$ (dark blue) mice. Scale bars 20 μm (a,b,f-i) 200 μm (c,d,o-q, s-u). (**e,j,r,v**) The number at the base of each chart bar is n and represents number of mice. p-values by One Way ANOVA (**e, r, v**), Student's T-test (**j, l, m**). Error bars are SEM. Images are representative of at least three separate experiments.